DOI: 10.1002/ejic.201100289

A Tale of Two Polymorphs – Growth and Characterization of α-$LnNiGa_4$ (Ln = Y, Gd–Yb) and β-$LnNi_{1-x}Ga_4$ (Ln = Tb–Er)

Melissa C. Menard,[a] Brenton L. Drake,[a] Gregory T. McCandless,[a] Kandace R. Thomas,[a] Richard D. Hembree,[a] Neel Haldolaarachchige,[b] John F. DiTusa,[b] David P. Young,[b] and Julia Y. Chan*[a]

Dedicated to Professor John D. Corbett on the occasion of his 85th birthday

Keywords: Crystal growth / Magnetic properties / Intermetallic phases / Gallium

The single crystals of two polymorphs of $LnNiGa_4$, namely, the orthorhombic α-$LnNiGa_4$ (Ln = Y, Gd–Yb) and, a new polymorph, the tetragonal β-$LnNi_{1-x}Ga_4$ (Ln = Tb–Er), were successfully grown by using the self-flux method. α-$LnNiGa_4$ (Ln = Y, Gd–Yb) is isostructural to $YNiAl_4$ and can be described as an edge-sharing polyhedral of $Ni@Ga_7Ln_2$ (Ln = Y, Gd–Yb) along the *ac*-plane that is sandwiched between the square nets of the Ga atoms along the *b*-axis. The structure of β-$LnNi_{1-x}Ga_4$ (Ln = Tb–Er) is a distorted variant of the Ce_2NiGa_{10}-structure type with a Ni deficiency and multiple Ga split positions and is structurally related to $YNiGa_3Ge$. The magnetic data for β-$LnNi_{1-x}Ga_4$ (Ln = Tb–Er) and the transport properties for α-$LnNiGa_4$ (Ln = Y, Gd–Tm) and β-$LnNi_{1-x}Ga_4$ (Ln = Tb–Er) are reported. Antiferromagnetic correlations are observed in the magnetic susceptibility of β-$LnNi_{1-x}Ga_4$ (Ln = Tb–Er), where the magnetic transitions occurred below 7 K and with effective moments that are consistent with free Ln^{3+} ions.

Introduction

The defects and imperfections in crystalline materials are generally referred to as disorder, which is commonly considered an undesirable quality. However, structural disorder may be a desirable property when one is searching for new materials that have exotic properties. The disorder can be used as a tunable parameter when the atomic sizes, coordination preferences, and electronegativity differences can be varied by substituting elements into a given structure. The demonstration of this type of control often involves tuning at the edge of the structural stability and careful adjustment of the synthetic parameters in order to grow phases that have inherent structural disorder. The systems that contain disordered Ga-networks exhibit a wide variety of phenomena that include charge density wave formation in $LnCo_xGa_3Ge$ (Ln = Y, Gd),[1,2] spin density wave formation in $U_3Ga_2Si_3$,[3] the observation of zero thermal expansion of YbGaGe,[4] negative thermal expansion of $YbGa_{1+x}Ge_{1-x}$,[5] and spin glass behavior of $Ce_2Ag_{1-x}Ga_{10-y}$.[6] Unusual electronic and magnetic behavior may be due to the inhomogeneous electronic environment that surrounds the localized magnetic moments in structurally distorted networks. The structural modulation that was discovered in $LnCo_xGa_3Ge$ (Ln = Y, Gd) suggested that a charge density wave instability phase may be caused by modulations in its structure.[1,2] Atomic site disorder can also affect the magnetic properties of materials. Examples of this include $Ce_2Ag_{1-x}Ga_{10-y}$, which exhibits a time-dependent magnetism that has been tentatively associated with a disorder-induced spin glass-like coupling of the Ce^{3+} moments with long-range antiferromagnetic ordering that only develops below 3 K.[6] This behavior is similar to the spin glass behavior that was observed in Ce_2CuSi_3 and Ce_2CuGe_3, where the atomic site disorder, which is a mixture of the transition metal (Cu) and the main group metal (Si or Ge), is analogous to applying chemical pressure in order to alter the electronic environment around the Ce^{3+} moments.[7,8] Similarly, the disorder and Ag substitution suppressed the magnetic ordering of $Gd(Ag,Al,Si)_2$ by 9 K as compared to that of the parent $Gd(Al,Si)_2$.[9] Other examples of physical properties that are controlled by disorder include the heavy fermion metal, $CePd_2Al_3$, where the random occupation of two of the Al sites leads to a varying electronic environment around the Ce^{3+} moments, which prevents long-range magnetic order.[10] These examples illustrate the effects of atomic disorder on the magnetic ordering.

[a] Department of Chemistry, Louisiana State University, Baton Rouge, Louisiana, 70803, USA
Fax: +1-225-578-3458
E-mail: jchan@lsu.edu
[b] Department of Physics and Astronomy, Louisiana State University, Baton Rouge, Louisiana, 70803, USA

As part of our search for highly correlated Ce and Yb systems, we were especially interested in studying the interplay between the Kondo effect and RKKY interactions in a series of isostructural materials. The title phases, namely, orthorhombic α-$LnNiGa_4$ (Ln = Y, Gd–Yb) and tetragonal β-$LnNi_{1-x}Ga_4$ (Ln = Tb–Er), were synthesized serendipitously while attempting to grow the latter lanthanide analogues of the Sm_2NiGa_{12}-structure type.[11] The structure and properties of the orthorhombic α-$LnNiGa_4$ (Ln = Y, Nd, Sm, and Gd–Lu) have been previously reported.[12] The structure was characterized as isostructural to $YNiAl_4$ by X-ray powder diffraction of the polycrystalline arc-melted samples.[13] The magnetic susceptibility, which was measured over 78 to 300 K, indicated antiferromagnetic correlations in the Nd and Gd systems and positive Weiss temperatures (θ_W) for the Tb to Tm systems. Three of the analogues, namely, the Y, Yb, and Lu systems, exhibited diamagnetic behavior while the Sm analogue showed Van Vleck paramagnetism. All of the analogues indicated that Ni does not carry a moment in α-$LnNiGa_4$ (Ln = Y, Nd, Sm, and Gd–Lu). The tetragonal β-$LnNi_{1-x}Ga_4$ is a new defect variant of the Ce_2NiGa_{10}-structure type.[14] In this paper we report on the growth, structural characterization, and transport properties of the single crystals of the orthorhombic α-$LnNiGa_4$ (Ln = Y, Gd–Yb) and tetragonal β-$LnNi_{1-x}Ga_4$ (Ln = Tb–Er), as well as on the magnetic properties of the tetragonal β-$LnNi_{1-x}Ga_4$ (Ln = Tb–Er).

Results and Discussion

Synthesis of α-$LnNiGa_4$ (Ln = Y, Gd–Yb) and β-$LnNi_{1-x}Ga_4$ (Ln = Tb–Er)

The reaction profiles for the growth of α-$LnNiGa_4$ (Ln = Y, Gd–Yb)[12] and β-$LnNi_{1-x}Ga_4$ (Ln = Tb–Er) (Figure 1) are very similar to that of Ln_2NiGa_{12} (Ln = Pr, Nd, Sm).[15] The differences in the cooling sequences resulted in the growth of α-$LnNiGa_4$ or a mixture of α-$LnNiGa_4$ and β-$LnNi_{1-x}Ga_4$. All of the samples were heated to 1423 K at 170 K/h and were annealed at 1423 K for 24 h.

The cooling sequence of α-$LnNiGa_4$ (Ln = Y, Gd–Yb) involved rapid cooling (ca. 200 K/h) of the sample to 973 K, followed by slow cooling (8 K/h) to 873 K, and then the sample was maintained at 873 K for 2 days prior to centrifugation (Figure 1). The growth of large single crystals of α-$TmNiGa_4$, however, required the elimination of the rapid cooling step in the temperature profile (red line in Figure 1). After the sample was maintained at 1423 K for 24 h, α-$TmNiGa_4$ was slow cooled from 1423 K to 873 K at 10 K/h and then kept at 873 K for 2 days before centrifugation. All of the Ln = Y, Gd, Tm–Yb crystals that were grown by the rapid cooling (ca. 200 K/h) of the sample to 773 K, followed by slow cooling (8 K/h) to 723 K, resulted in three different phases, namely, α-$LnNiGa_4$ (Ln = Y, Gd, Tm, Yb), $BaAl_4$-type $Ln(Ni,Ga)_4$,[16] and an unknown phase where the stoichiometry was found to be $LnNi_{1.3(1)}Ga_{4.3(1)}$ by elemental analysis. The optimal growth conditions for the orthorhombic phase are consistent with the initial reports for the formation of orthorhombic α-$LnNiGa_4$ (Ln = Y, Gd–Yb) by means of the peritectic reaction at 1151 K.[17] The slow cooling of the sample below 723 K led to the formation of multiple phases, instead of the α-$LnNiGa_4$ (Ln = Y, Gd–Yb) phase, that included $PuGa_6$-type $LnGa_6$ (Ln = Y, Gd–Yb)[18] and $BaAl_4$-type $Ln(Ni,Ga)_4$ systems,[16] and an unknown phase where the stoichiometry was found to be $LnNi_{1.3(1)}Ga_{4.3(1)}$ (Ln = Y, Gd–Yb) by elemental analysis.

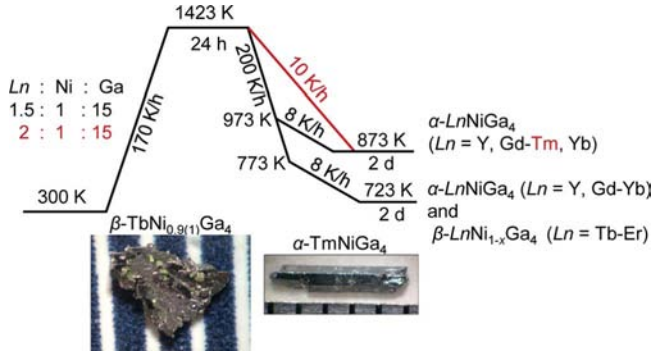

Figure 1. The growth profiles for α-$LnNiGa_4$ (Ln = Y, Gd–Yb) and β-$LnNi_{1-x}Ga_4$ (Ln = Tb–Er) are shown with the crystal pictures of α-$TmNiGa_4$ and β-$TbNi_{0.9(1)}Ga_4$. The synthesis ratio and the profile adjustments that were required for the growth of the large crystals of α-$TmNiGa_4$ are indicated in red. The surface roughness is due to etching and crystal deformities that were incurred while separating the crystals.

β-$LnNi_{1-x}Ga_4$ (Ln = Tb–Er) was grown by the rapid cooling (ca. 200 K/h) of the sample to 773 K and then slow cooling of the sample (8 K/h) to 723 K. After 2 days at 773 K, each sample was inverted and centrifuged to remove the excess Ga flux. All of the crystal growths for β-$LnNi_{1-x}Ga_4$ (Ln = Tb–Er) yielded approximately 15% of the α-$LnNiGa_4$ (Ln = Tb–Er) impurity phase and, when a sample of β-$LnNi_{1-x}Ga_4$ (Ln = Tb–Er) was allowed to cool slowly (10 K/h) from 823 K to 723 K, the product contained approximately 60% β-$LnNi_{1-x}Ga_4$ (Ln = Tb–Er) and 40% α-$LnNiGa_4$ (Ln = Tb–Er).[12] These growth experiments indicated that the two-step cooling sequence, which involved rapid cooling of the sample to 773 K followed by slow cooling of the sample to 723 K, is important for the reduction of the impurity phase.

Although the orthorhombic α-$LnNiGa_4$ (Ln = Tb–Er)[12] and tetragonal β-$LnNi_{1-x}Ga_4$ (Ln = Tb–Er) phases were grown concurrently, they were easily separated by their crystal morphologies. As shown in Figure 1, the orthorhombic α-$LnNiGa_4$ phase grows as rods that are approximately 6 mm in length while the tetragonal β-$LnNi_{1-x}Ga_4$ phase grows as plate-like aggregates that are up to 2 mm × 1 mm × 0.025 mm in size. The crystals of both of the polymorphs did not show signs of degradation in air and dilute HCl was used to remove the excess Ga flux from the surface of the crystals. The phase of each of the crystals that were used for the physical property measurements was identified by means of single-crystal X-ray diffraction.

EurJIC European Journal of Inorganic Chemistry

Structure Determination

The preliminary lattice determination for the α-$LnNiGa_4$ (Ln = Y, Gd–Yb) systems indicated an orthorhombic cell for each phase with $a \approx 4$ Å, $b \approx 15$ Å, $c \approx 6$ Å, $V \approx 360$ Å^3 and a point group symmetry of *mmm*. The atomic parameters for $YNiAl_4$ were used as the starting values for the refinement.[13] The atomic positions and the interatomic distances are provided in Tables 1, 2, and 3.

Table 1. Positional and atomic displacement parameters for α-$LnNiGa_4$ (Ln = Y, Gd–Yb) at 298 K.

Atom		x	y	z	U_{eq} [Å^2][a]
α-$YNiGa_4$					
Y	4*c*	0	0.61842(6)	1/4	0.0064(3)
Ni1	4*c*	0	0.27492(8)	1/4	0.0098(4)
Ga1	4*a*	0	0	0	0.0101(3)
Ga2	4*c*	0	0.42719(8)	1/4	0.0108(3)
Ga3	8*f*	0	0.81393(5)	0.05148(13)	0.0077(3)
α-$GdNiGa_4$					
Gd	4*c*	0	0.61739(3)	1/4	0.0087(2)
Ni1	4*c*	0	0.27550(9)	1/4	0.0106(4)
Ga1	4*a*	0	0	0	0.0101(3)
Ga2	4*c*	0	0.42714(8)	1/4	0.0123(3)
Ga3	8*f*	0	0.81353(5)	0.05164(14)	0.0114(3)
α-$TbNiGa_4$					
Tb	4*c*	0	0.61744(3)	1/4	0.0076(2)
Ni1	4*c*	0	0.27510(9)	1/4	0.0109(4)
Ga1	4*a*	0	0	0	0.0114(3)
Ga2	4*c*	0	0.42689(9)	1/4	0.0120(3)
Ga3	8*f*	0	0.81371(6)	0.05107(14)	0.0100(3)
α-$DyNiGa_4$					
Dy	4*c*	0	0.61803(5)	1/4	0.0082(3)
Ni1	4*c*	0	0.27498(16)	1/4	0.0121(6)
Ga1	4*a*	0	0	0	0.0117(5)
Ga2	4*c*	0	0.42764(14)	1/4	0.0124(5)
Ga3	8*f*	0	0.81413(9)	0.0508(2)	0.0105(4)
α-$HoNiGa_4$					
Ho	4*c*	0	0.61873(4)	1/4	0.0076(2)
Ni1	4*c*	0	0.27497(11)	1/4	0.0117(4)
Ga1	4*a*	0	0	0	0.0116(4)
Ga2	4*c*	0	0.42793(10)	1/4	0.0115(4)
Ga3	8*f*	0	0.81444(6)	0.05087(17)	0.0098(3)
α-$ErNiGa_4$					
Er	4*c*	0	0.61926(4)	1/4	0.0226(4)
Ni1	4*c*	0	0.27482(13)	1/4	0.0259(5)
Ga1	4*a*	0	0	0	0.0267(5)
Ga2	4*c*	0	0.42831(13)	1/4	0.0267(5)
Ga3	8*f*	0	0.81470(7)	0.05092(18)	0.0240(4)
α-$TmNiGa_4$					
Tm	4*c*	0	0.61995(4)	1/4	0.0074(3)
Ni1	4*c*	0	0.27442(12)	1/4	0.0100(5)
Ga1	4*a*	0	0	0	0.0109(4)
Ga2	4*c*	0	0.42891(12)	1/4	0.0109(4)
Ga3	8*f*	0	0.81497(7)	0.05095(19)	0.0086(4)
α-$YbNiGa_4$					
Yb	4*c*	0	0.62066(5)	1/4	0.0064(4)
Ni1	4*c*	0	0.27698(15)	1/4	0.0072(6)
Ga1	4*a*	0	0	0	0.0105(5)
Ga2	4*c*	0	0.42952(14)	1/4	0.0105(5)
Ga3	8*f*	0	0.81449(9)	0.0501(2)	0.0075(4)

[a] U_{eq} is defined as one third of the trace of the orthogonalized $\mathbf{U}_{ij}$ tensor.

The preliminary lattice determination for the β-$LnNi_{1-x}Ga_4$ (Ln = Tb–Er) systems indicated a tetragonal cell for each phase with $a \approx 4$ Å, $c \approx 23$ Å, $V \approx 370$ Å^3 and a point group symmetry of 4/*mmm*. The data were collected on the single-crystals of β-$LnNi_{1-x}Ga_4$ (Ln = Tb–Er) at 298 and 100 K in order to investigate the nature of the disorder at the Ni2, Ga2, Ga3, Ga4, and Ga5 sites. In this paper we have reported the 100 K data since the structural model did not change with temperature, which is consistent with statistical disorder. Each of the data collections encompassed a full sphere of reciprocal space. The atomic positions of $YNiGa_3Ge$[19] were used as the starting model. The atomic positions and the interatomic distances are provided in Tables 4 and 5.

Table 2. Interatomic distances [Å] for α-$LnNiGa_4$ (Ln = Y, Gd–Dy).

		α-$YNiGa_4$	α-$GdNiGa_4$	α-$TbNiGa_4$	α-$DyNiGa_4$
Ln–Ln	(×2)	4.076(5)	4.093(5)	4.080(5)	4.069(5)
Ln–Ga1	(×4)	3.1774(18)	3.1807(18)	3.1716(18)	3.1678(18)
Ln–Ga2		2.9153(18)	2.9213(16)	2.9127(17)	2.900(2)
Ln–Ga2	(×2)	3.349(2)	3.345(2)	3.341(2)	3.338(2)
Ln–Ga3	(×4)	3.020(2)	3.036(2)	3.025(2)	3.011(2)
Ln–Ga3	(×2)	3.2520(15)	3.2799(13)	3.2703(14)	3.2575(18)
Ln–Ni	(×2)	3.138(2)	3.175(2)	3.158(2)	3.139(3)
Ni–Ga2		2.3214(19)	2.328(2)	2.4612(8)	2.325(3)
Ni–Ga3	(×2)	2.3591(17)	2.4021(17)	2.280(12)	2.387(2)
Ni–Ga3	(×4)	2.490(2)	2.493(2)	2.491(2)	2.487(2)
Ni–Ni	(×4)	3.932(2)	3.939(2)	3.931(2)	3.921(2)

Table 3. Interatomic distances [Å] for α-$LnNiGa_4$ (Ln = Ho–Yb).

		α-$HoNiGa_4$	α-$ErNiGa_4$	α-$TmNiGa_4$	α-$YbNiGa_4$
Ln–Ln	(×2)	4.062(5)	4.057(4)	4.0478(2)	4.0850(4)
Ln–Ga1	(×4)	3.1692(18)	3.1695(15)	3.1709(4)	3.1960(5)
Ln–Ga2		2.8973(19)	2.891(2)	2.8825(19)	2.923(2)
Ln–Ga2	(×2)	3.343(2)	3.347(2)	3.3578(5)	3.338(6)
Ln–Ga3	(×4)	3.003(2)	2.9973(19)	2.9913(9)	2.9929(10)
Ln–Ga3	(×2)	3.2442(15)	3.2325(16)	3.2186(12)	3.2358(16)
Ln–Ni	×(2)	3.123(2)	3.108(2)	3.0868(14)	3.1440(18)
Ni–Ga2		2.323(2)	2.324(3)	2.331(3)	2.332(3)
Ni–Ga3	(×2)	2.3891(19)	2.389(2)	2.3889(16)	2.3997(19)
Ni–Ga3	(×4)	2.485(2)	2.4845(19)	2.4842(8)	2.4876(9)
Ni–Ni	(×4)	3.921(2)	3.920(2)	3.9205(5)	3.9254(7)

Anomalous atomic displacement parameters and unusual residual electron densities were observed for the Ni2 (4*e*), Ga2 (4*e*), and Ga4 (4*d*) positions in the initial model of β-$LnNi_{1-x}Ga_4$ (Ln = Tb–Ho). Due to the unrealistic interatomic distances that were found between Ni2 and Ga3 (ca. 1.76 Å), the occupancy of the Ni2 (4*e*) site was refined freely and found to be approximately 40% for each of the analogues. In a similar manner to the refinement of the Ge position in $YNiGa_3Ge$,[19] the Ga2 (4*e*) was refined as a split position with approximately 50% occupancy for the Ga2 (4*e*) and Ga3 (4*e*) sites for each of the analogues. The refinement of the Ga (4*e*) site as a single site resulted in a large atomic displacement parameter and R values that were approximately 15% higher than split site model. The disorder observed at the Ni2, Ga2, and Ga3 sites is similar to that found at equivalent sites in $YNiGa_3Ge$. An additional disordered area that was not seen in $YNiGa_3Ge$

Table 4. Positional and atomic displacement parameters for β-$LnNi_{1-x}Ga_4$ (Ln = Tb–Er) at 100 K.

Atom		x	y	z	Occ.[a]	U_{eq} [Å^2][b]
β-$TbNi_{0.9(1)}Ga_4$						
Tb	4*e*	0	0	0.14717(3)	1.00	0.0159(5)
Ni1	2*a*	0	0	0	1.00	0.0162(9)
Ni2	4*e*	0	0	0.2827(3)	0.43(2)	0.0343(19)
Ga1	8*g*	1/2	0	0.44519(7)	1.00	0.0198(6)
Ga2	4*e*	0	0	0.3819(3)	0.51(5)	0.0216(13)
Ga3	4*e*	0	0	0.3567(4)	0.49(5)	0.0236(16)
Ga4	4*d*	0	1/2	3/4	0.38(2)	0.033(2)
Ga5	16*n*	0	0.629(4)	0.7372(6)	0.15(2)	0.051(3)
β-$DyNi_{0.9(1)}Ga_4$						
Dy	4*e*	0	0	0.14754(2)	1.00	0.0059(3)
Ni1	2*a*	0	0	0	1.00	0.0056(6)
Ni2	4*e*	0	0	0.2821(2)	0.43(2)	0.0264(13)
Ga1	8*g*	1/2	0	0.44471(5)	1.00	0.0085(4)
Ga2	4*e*	0	0	0.3801(3)	0.50(5)	0.0133(9)
Ga3	4*e*	0	0	0.3539(2)	0.50(5)	0.0092(9)
Ga4	4*d*	0	1/2	1/4	0.60(2)	0.0287(11)
Ga5	16*n*	0	0.626(4)	0.7381(7)	0.10(2)	0.044(3)
β-$HoNi_{0.9(1)}Ga_4$						
Ho	4*e*	0	0	0.14766(3)	1.00	0.0171(4)
Ni1	2*a*	0	0	0	1.00	0.0164(7)
Ni2	4*e*	0	0	0.2821(3)	0.43(2)	0.0390(17)
Ga1	8*g*	1/2	0	0.55563(6)	1.00	0.0194(4)
Ga2	4*e*	0	0	0.3790(4)	0.49(5)	0.0279(12)
Ga3	4*e*	0	0	0.3535(2)	0.51(5)	0.0184(11)
Ga4	4*d*	0	1/2	3/4	0.40(2)	0.0234(19)
Ga5	16*n*	0	0.592(5)	0.7437(9)	0.15(2)	0.056(4)
β-$ErNi_{0.8(1)}Ga_4$						
Er	4*e*	0	0	0.14817(2)	1.00	0.0083(3)
Ni1	2*a*	0	0	0	1.00	0.0066(5)
Ni2	4*e*	0	0	0.2835(3)	0.32(2)	0.0113(11)
Ga1	8*g*	1/2	0	0.44385(5)	1.00	0.0107(3)
Ga2	4*e*	0	0	0.3831(4)	0.30(3)	0.0130(13)
Ga3	4*e*	0	0	0.35379(17)	0.70(3)	0.0158(6)
Ga4	4*d*	0	1/2	3/4	0.84(2)	0.0332(8)
Ga5	16*n*	0	0.629(8)	0.7411(15)	0.04(2)	0.028(6)

[a] Occupancy. [b] U_{eq} is defined as one third of the trace of the orthogonalized $\mathbf{U}_{ij}$ tensor.

Table 5. Interatomic distances [Å] for β-$LnNi_{1-x}Ga_4$ (Ln = Tb–Er).

		β-$TbNi_{0.9(1)}Ga_4$	β-$DyNi_{0.9(1)}Ga_4$	β-$HoNi_{0.9(1)}Ga_4$	β-$ErNi_{0.8(1)}Ga_4$
Ln–Ln	(×4)	4.1980(6)	4.1790(6)	4.1680(2)	4.1620(6)
Ln–Ga1	(×4)	3.0386(13)	3.0206(2)	3.0058(11)	2.9988(9)
Ln–Ga2	(×4)	3.0479(17)	3.0264(3)	3.013(2)	3.033(2)
Ln–Ga3	(×4)	2.9699(4)	2.9552(3)	2.9473(2)	2.9433(3)
Ln–Ga4	(×4)	3.2233(6)	3.1993(2)	3.1852(5)	3.1686(4)
Ln–Ga5	(×8)	3.047(10)	3.0378(2)	3.10(2)	3.06(3)
Ln–Ga5	(×4)	3.161(12)	3.1232(3)	3.07(2)	3.02(3)
Ln–Ga5	(×4)	3.813(10)	3.7624(3)	3.55(2)	3.69(2)
Ni1–Ga1	(×8)	2.4710(9)	2.4648(3)	2.4612(8)	2.4630(7)
Ni2–Ga2		2.360(10)	2.3172(3)	2.280(12)	2.33(1)
Ni2–Ga3		1.760(12)	1.6977(3)	1.681(8)	1.649(8)
Ni2–Ga4	(×4)	2.239(3)	2.2231(3)	2.217(2)	2.224(2)
Ni2–Ga5	(×8)	2.423(10)	2.3928(3)	2.304(9)	2.368(16)
Ni2–Ga5	(×4)	1.628(17)	1.6343(2)	1.81(2)	1.65(3)
Ni2–Ga5	(×4)	2.683(10)	2.6593(4)	2.54(2)	2.680(7)

was observed at the Ga4 (4*d*) site in β-$LnNi_{1-x}Ga_4$ (Ln = Tb–Er). The Ga4 (4*d*) site was refined as a split between the Ga4 (4*d*) and Ga5 (16*n*) sites for the Ln = Tb–Ho analogues. The refinement of Ga4 as a fully occupied site resulted in a large prolate thermal ellipsoid for Ga4 and a residual electron density peak (ca. 6 e/Å^3) at a distance of approximately 0.8 Å from Ga4. The short interatomic distances between the neighboring Ni2, Ga4, and Ga5 sites are consistent with the partially occupied model.

The occupancies of the disordered sites in β-$ErNi_{0.8(1)}Ga_4$ were noticeably different compared to those of β-$LnNi_{1-x}Ga_4$ (Ln = Tb–Ho). The Ni occupancy at the Ni2 site decreased from approximately 43% in β-$LnNi_{1-x}Ga_4$ (Ln = Tb–Ho) to approximately 32% in β-$ErNi_{0.8(1)}Ga_4$. In conjunction with the decrease of the Ni occupation at the Ni2 site, the occupation of Ga at the Ga4 (4*d*) site was much larger (ca. 84%) and that at the Ga5 (16*n*) site was much smaller (ca. 4%) when compared to those of β-$LnNi_{1-x}Ga_4$ (Ln = Tb–Ho). The split positions, Ga2 (4*e*) and Ga3 (4*e*), were approximately 30 and 70% occupied, respectively. The differences in the occupancies of the disordered sites illustrated the effects of the lanthanide contraction and also marked the end of the β-$LnNi_{1-x}Ga_4$ (Ln = Tb–Er) series due to the increasing structural instability with the decrease in the lanthanide size.

The disorder in the β-$LnNi_{1-x}Ga_4$ (Ln = Tb–Er) series is very similar to that found in the $LnMGa_3Ge$ (Ln = Y, Sm, Gd, Yb; M = Ni, Co) series,[19] which was attributed to the complex modulations in the $[NiGa]_2$ nets. The reciprocal lattice of $LnMGa_3Ge$ (Ln = Y, Sm, Gd, Tb, Er, Tm; M = Ni, Co) featured satellite reflections with incommensurate spacing due to the structural modulation in the $[MGa]_2$ nets in the *ab* plane that was seen in the electron diffraction.[2,19] Although β-$LnNi_{1-x}Ga_4$ (Ln = Tb–Er) is structurally very similar to $LnMGa_3Ge$, the symmetry forbidden, supercell reflections were not observed in the reciprocal lattice precession images from the single-crystal X-ray diffraction of β-$LnNi_{1-x}Ga_4$ (Ln = Tb–Er), where the data were collected at long integration times (150 s/°) without overflow scans.

Structure of α-$LnNiGa_4$ (Ln = Y, Gd–Yb) and β-$LnNi_{1-x}Ga_4$ (Ln = Tb–Er)

The structure of the α-$LnNiGa_4$ (Ln = Y, Gd–Yb) series, which is isostructural to $YNiAl_4$,[13] is built out of edge-sharing polyhedra of $Ni@Ga_7Ln_2$ (Ln = Y, Gd–Yb) along the *ac*-plane that is sandwiched between the square nets of the Ga atoms along the *b*-axis as shown in Figure 2.

β-$LnNi_{1-x}Ga_4$ (Ln = Tb–Er), which is the tetragonal polymorph, is a new, disordered variant of the Ce_2NiGa_{10}-structure type as shown in Figure 3a.[14] The linear intergrowth of Ce_2NiGa_{10} consists of $BaAl_4$-type $CeGa_4$ segments of the face-sharing tetragonal antiprisms, $^2_\infty[Ce_{4/8}Ga_{4/4}]_2$, and CaF_2-type Ga_2Ni segments of the face-sharing rectangular prisms, $^2_\infty[Ga_{8/4}Ni]$.[20,21] The combination of these two segments yields $2CeGa_4 + Ga_2Ni = Ce_2NiGa_{10}$. In the case of β-$LnNi_{1-x}Ga_4$ (Ln = Tb–Er), the distorted $BaAl_4$-type segment consists of $^2_\infty[Ln_{4/8}(Ni,Ga)_{4/4}]_2 = LnNi_{1-x}Ga_3$ tetragonal antiprisms, where *x*

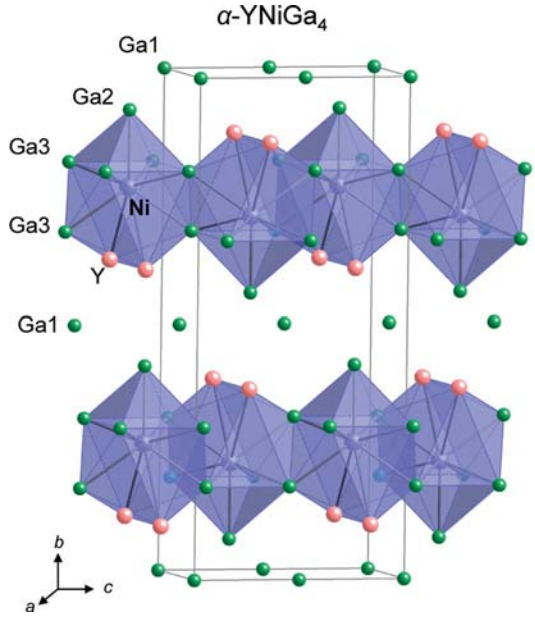

Figure 2. The crystal structure for α-YNiGa$_4$ is shown with the Y, Ni, and Ga atoms represented by the pink, purple, and green spheres, respectively.

represents an approximately 60% Ni deficiency at the 4*e* site for Ln = Tb–Ho and an approximately 70% Ni deficiency for β-ErNi$_{0.8(1)}$Ga$_4$, and the CaF_2-type segment consists of the face-sharing rectangular prisms of $^2_\infty$[NiGa$_{8/4}$] = NiGa$_2$. The combination of these two segments yields 2LnNi$_{1-x}$Ga$_3$ + NiGa$_2$ = Ln$_2$Ni(Ni$_{2-2x}$Ga$_8$).

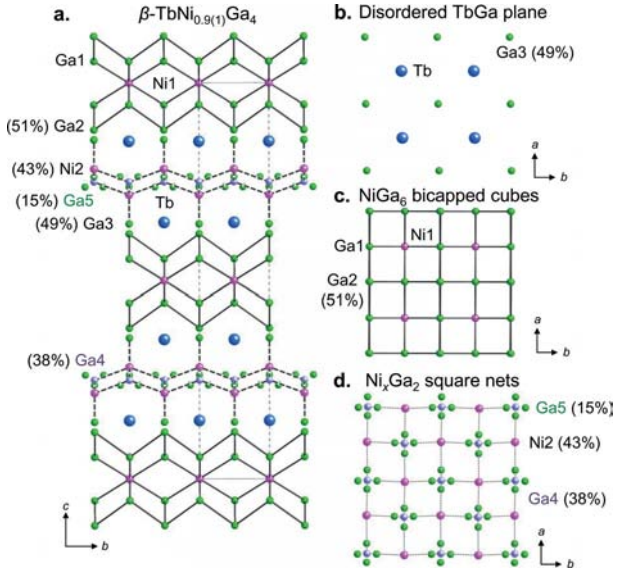

Figure 3. (a) The crystal structure for β-TbNi$_{0.9(1)}$Ga$_4$ is shown with the Tb and Ni atoms represented by the blue and pink spheres, respectively. The Ga atoms are represented by the green and purple spheres to highlight the disorder in this phase. (b) The disordered TbGa plane where Ga3 is 49% occupied. (c) The NiGa$_6$ bicapped cubes where Ga2 is 51% occupied. (d) The puckered Ni$_x$Ga$_2$ square nets where Ni2, Ga4, and Ga5 are 43%, 38%, and 15% occupied, respectively. The dashed lines indicate the bonding between the disordered sites and, unless otherwise indicated, the sites that are 100% occupied.

This particular distorted variant of the Ce$_2$NiGa$_{10}$-structure type[14] is isotypic with YNiGa$_3$Ge[19] and Ce$_2$NiAl$_{6-x}$Ge$_{4-y}$.[22] The structure of β-LnNi$_{1-x}$Ga$_4$ (Ln = Tb–Er) can be described as a stacking of the LnGa planes with Ga occupational disorder, the NiGa$_6$ bicapped cubes with Ga occupational disorder on the capping sites, and the puckered Ni$_x$Ga$_2$ square nets with a split Ga position. The disordered LnGa plane, shown in Figure 3b, is defective and has only a 50% occupancy for the Ga3 site. The Ln–Ln interatomic distances are equal to the length of the crystallographic *a*-axis and are not within a typical bonding distance. The Ln–Ga3 interatomic distances are in good agreement with those found for the Ln–Ga binaries (Ln = Tb–Er).[23–25] The Ni1–Ga1 distances (Figure 3c) are consistent with the Ni–Ga atomic radii (ca. 2.49 Å)[26] and with the Ni–Ga binaries, which range from approximately 2.47 to 2.61 Å.[27–31] The NiGa$_6$ bicapped cubes (Figure 3c) are very similar to the bicapped MGa$_6$ (M = Ga or transition metal) cubes found in Ce$_2$NiGa$_{10}$,[14] Ln$_3$NiGa$_{10}$ (Ln = Ce–Nd),[32] Ce$_4$Ni$_{1.24}$Ga$_{17.76}$,[33] Sm$_2$NiGa$_{12}$,[11] Sm$_2$Ni(Ni$_x$Si$_{1-x}$)Al$_4$Si$_6$,[34] YNiGa$_3$Ge,[19] Ce$_2$NiAl$_{6-x}$Ge$_{4-y}$,[22] YbGa$_5$,[35] and Ce$_2$Ag$_{1-x}$Ga$_{10-y}$.[6] The puckered Ni$_x$Ga$_2$ square nets, which are approximately 43% occupied by Ni for Ln = Tb–Ho and approximately 32% occupied by Ni for Ln = Er, have Ni2–Ga interatomic distances that range from approximately 1.63 to 2.68 Å (Figure 3d). The shortest Ni2–Ga5 (ca. 1.6 Å) and Ni2–Ga4 (ca. 2.2 Å) interatomic distances are consistent with the partial occupancy of these sites, which yields the empty puckered square nets in approximately 57 to 68% of the unit cells. It is important to note that the shortest Ni2–Ga5 distance and all of the Ni2–Ga4 distances are shorter than expected, which indicated that when Ni2 is present in a unit cell the Ga4 or the closest Ga5 atoms are not present. There are two Ni sites in this structure. The structurally ordered Ni1 site (2*a*) is in a rectangular prismatic environment, whereas the occupationally-deficient Ni2 site (4*e*) is in a distorted, puckered square planar environment. In the ordered Ce$_2$NiGa$_{10}$ structure, the 4*e* site is occupied by Ga instead of Ni.

The Ln atoms in both α-LnNiGa$_4$ (Ln = Y, Gd–Yb) and β-LnNi$_{1-x}$Ga$_4$ (Ln = Tb–Er) occupy the channels of the NiGa-network and have no direct bonding interaction with either the Ni or the Ga atoms (ca. 3.0 Å). The Ln–Ln distances are larger in the β-LnNi$_{1-x}$Ga$_4$ (Ln = Tb–Er) analogue (ca. 4.17 Å) than in the α-LnNiGa$_4$ (Ln = Tb–Er) series (ca. 4.05 Å). The disorder in the local environment of the Ln in β-LnNi$_{1-x}$Ga$_4$ (Ln = Tb–Er) could be attributed to the varying local electronic environment of the Ln that manifests as magnetic frustration. The spin glass behavior observed in Ce$_2$Ag$_{1-x}$Ga$_{10-y}$,[6] Ce$_2$CuSi$_3$,[7] and Ce$_2$CuGe$_3$[8] has been attributed to such structural disorder in the local Ln^{3+} environments. Frustration due to the structural disorder in β-LnNi$_{1-x}$Ga$_4$ (Ln = Tb–Er) is consistent with the large discrepancy between T_N and θ_W in β-LnNi$_{1-x}$Ga$_4$ (Ln = Tb–Er), as shown in Table 6.

Table 6. Magnetic properties for β-$LnNi_{1-x}Ga_4$ (Ln = Tb–Er).

	T_N [K]	μ_{eff} [μ_B/mol] calcd.	μ_{eff} [μ_B/mol] exptl.	θ_W [K]	T [K]
β-$TbNi_{0.9(1)}Ga_4$	7	9.72	9.8(1)	–43.6(5)	25–300
β-$DyNi_{0.9(1)}Ga_4$	3.5	10.65	10.5(1)	–22.7(2)	25–300
β-$HoNi_{0.9(1)}Ga_4$	–	10.61	10.5(2)	–14.1(5)	20–300
β-$ErNi_{0.8(1)}Ga_4$	7	9.58	8.9(2)	–6.1(1)	20–300

The Ni environment in the α-$LnNiGa_4$ (Ln = Y, Gd–Yb) series is unique and has short contacts between the two Ln atoms (ca. 3.1 Å) and the 7 Ga atoms (ca. 2.4 Å). The two Ni environments in β-$LnNi_{1-x}Ga_4$ (Ln = Tb–Er) are very different and make for an interesting comparison between the coordination environment and the degree of structural disorder in this polymorph. Ni1 (2*a*) is in an ordered rectangular prismatic environment and Ni2 (4*e*) is in a distorted square planar environment. The Ni2–Ga distances that were observed in β-$LnNi_{1-x}Ga_4$ (Ln = Tb–Er) range between approximately 1.6 (when Ni2 is absent) and 2.5 Å (when Ni2 is present). In the ordered parent structure type, Ce_2NiGa_{10}, Ga occupies the equivalent position that Ni2 occupies in β-$LnNi_{1-x}Ga_4$ (Ln = Tb–Er). When Ni is present at the 4*e* site in β-$LnNi_{1-x}Ga_4$ (Ln = Tb–Er), the disorder observed in the Ni2 environment can be attributed to the partial occupancy of the Ni and the split Ga positions (4*d*/16*n*), which demonstrates a response to the presence or absence of Ni. The decreasing occupancy at the Ni2 position resulted in the increased occupancy of Ga4 and the decreased occupancy of Ga5, which resulted in shorter Ni2–Ga4 and longer Ni2–Ga5 distances compared to those of the other β-$LnNi_{1-x}Ga_4$ (Ln = Tb–Ho) analogues. The degree of disorder and the observation that the β-$ErNi_{0.8(1)}Ga_4$ analogue showed a notable decrease in occupancy at the Ni2 position, coupled with all of the unsuccessful attempts to grow a β-$TmNi_{1-x}Ga_4$ analogue, suggested that β-$ErNi_{0.8(1)}Ga_4$ is the terminal stable member. This observation is consistent with the lanthanide contraction. As the 4*e* – 4*d*/16*n* (Ni2 – Ga4/Ga5) environment in β-$LnNi_{1-x}Ga_4$ is limited in its degree of disorder, the Ga4/Ga5 positions become increasingly restricted, which effectively renders Ni incapable of populating the 4*e* position in the β-$TmNi_{1-x}Ga_4$ analogue.

Magnetic and Transport Properties

The temperature dependent magnetic susceptibility, χ_m, of β-$LnNi_{1-x}Ga_4$ (Ln = Tb–Er), which was measured under zero-field-cooled conditions from 2 to 300 K with an applied field of 0.1 T perpendicular to the direction of the plate, is shown in Figure 4 and the inverse susceptibility, χ_m^{-1}, for the same series is shown in the inset of Figure 4. All of the analogues, Tb–Er, were fitted with a modified Curie–Weiss equation of the form: $\chi(T) = \chi_0 + C/(T - \theta_W)$, where C is the Curie constant, θ_W is the Weiss temperature [K], and χ_0 is a constant, which is representative of any Larmor diamagnetic, Pauli paramagnetic, and background contributions to the magnetic susceptibility. In all of the cases, the modified Curie–Weiss equation was fitted over the linear region of χ_m^{-1}. A summary of the magnetic properties of β-$LnNi_{1-x}Ga_4$ (Ln = Tb–Er), including the T_N, μ_{eff} (calculated and experimental), θ_W, and fit range is given in Table 6. The crystals grew as plate-like aggregates and the directions of the applied field were assigned as the *c*-axis being perpendicular to the plates for β-$LnNi_{1-x}Ga_4$ (Ln = Tb–Er).

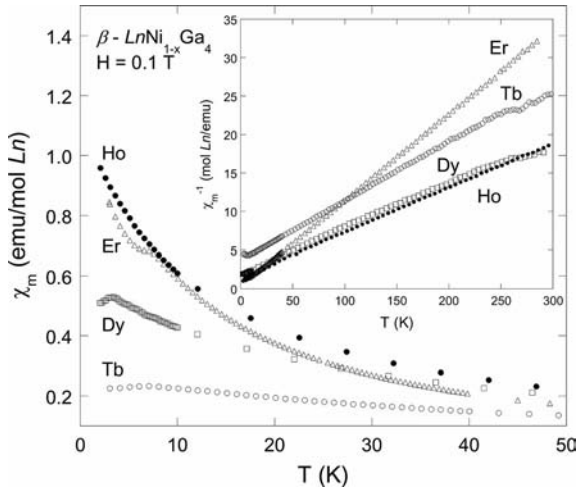

Figure 4. The magnetic susceptibility, χ_m = M/H [emu/mol Ln], as a function of temperature, T [K], with an applied field of H = 0.1 T for β-$TbNi_{0.9(1)}Ga_4$ (open circles), β-$DyNi_{0.9(1)}Ga_4$ (open squares), β-$HoNi_{0.9(1)}Ga_4$ (closed circles), and β-$ErNi_{0.8(1)}Ga_4$ (open triangles). The inverse magnetic susceptibility, χ_m^{-1} = H/M [mol Ln/emu], is shown in the inset.

β-$LnNi_{1-x}Ga_4$ (Ln = Tb, Dy, and Er) undergoes an antiferromagnetic transition (T_N) at approximately 7, 3.5, and 7 K, respectively, while the Ho analogue remained paramagnetic down to 2 K with H = 0.1 T. The inverse magnetic susceptibility, $\chi_m^{-1}(T)$ is shown in the inset of Figure 4. Above 20 K for $H \| c$, the series exhibited paramagnetic Curie–Weiss type behavior. The magnetic properties of β-$TbNi_{0.9(1)}Ga_4$ are similar to those of $TbNiGa_3Ge$ ($T_N \approx 5$ K and observed $\mu_{sat} \approx 3\ \mu_B$/mol).[19] The fitting of the data above 25 K for Tb and Dy and above 20 K for Ho and Er resulted in θ_W = –43.6(5), –22.7(2), –14.1(5), and –6.1(1) K for Tb, Dy, Ho, and Er, respectively. The negative θ_W values indicated that antiferromagnetic coupling was predominant and these values were consistent with the ordering that was observed for $TbNi_{0.9(1)}Ga_4$, $DyNi_{0.9(1)}Ga_4$, and $ErNi_{0.9(1)}Ga_4$. The frustration values, $|\theta_W|/T_N$, of 2–5 are considered typical for an antiferromagnetic system.[36] The frustration parameters, 6.2, 6.5, > 10, and 0.9 for the Tb, Dy, Ho, and Er analogues, respectively, indicated an increase in the frustration across the β-$LnNi_{0.9(1)}Ga_4$ (Ln = Tb–Ho) series and a decrease in the magnetic frustration in β-$ErNi_{0.8(1)}Ga_4$.[36] The decrease in the magnetic frustration on moving across the series β-$LnNi_{1-x}Ga_4$ (Ln = Tb, Dy, and Er) is consistent with the decrease in the structural frustration, as seen by the increase in the Ln–Ga4/Ga5 interatomic distances when β-$HoNi_{0.9(1)}Ga_4$ and β-$ErNi_{0.8(1)}Ga_4$ are compared. As mentioned above, the disorder in the local environment of

the Ln in β-LnNi$_{1-x}$Ga$_4$ (Ln = Tb–Er) could be attributed to the varying local electronic environment of the Ln, which manifests as magnetic frustration. Frustration due to structural disorder in β-LnNi$_{1-x}$Ga$_4$ (Ln = Tb–Er) is consistent with the large discrepancy between T_N and θ_W in β-LnNi$_{1-x}$Ga$_4$ (Ln = Tb–Er), as shown in Table 6.

The magnetic moments recovered, 9.8(1), 10.5(1), 10.5(2), and 8.9(2) μ_B/mol for the Tb, Dy, Ho, and Er analogues of β-LnNi$_{1-x}$Ga$_4$, respectively, were in good agreement with the calculated spin-only effective moments of 9.72, 10.65, 10.61, and 9.5 μ_B/mol for the trivalent Tb, Dy, Ho, and Er, respectively. In all of the cases, the recovered moment is reflective of the respective Ln^{3+} (Ln = Tb–Er) moment, which indicated that the Ni atoms do not show a localized magnetic moment and their contribution to the magnetism is diamagnetic. In addition, the relationship between θ_W [K] and the de Gennes factor for the α-LnNiGa$_4$ (Ln = Gd – Yb) series, as obtained by Romaka et al.,[12] and for the β-LnNi$_{1-x}$Ga$_4$ (Ln = Tb–Er) series, as obtained from this work, is shown in Figure 5. The trend for the β-LnNi$_{1-x}$Ga$_4$ (Ln = Tb–Er) series is similar to that of the α-LnNiGa$_4$ (Ln = Gd – Yb) series, which indicate that the magnetism of both the α-LnNiGa$_4$ and β-LnNi$_{1-x}$Ga$_4$ phases is due to de Gennes scaling.[12] The similarity in the scaling between the two polymorphs was expected as the nearest Ln–Ln distances are similar.

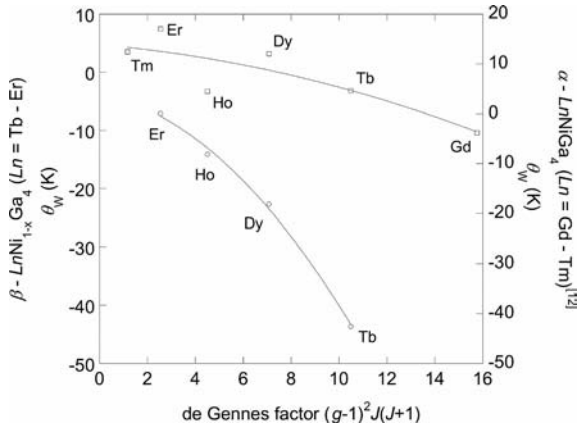

Figure 5. The variation of θ_W [K] as a function of the Ln–Ln interatomic distances for the α-LnNiGa$_4$ (Ln = Gd – Tm, open squares) series as obtained from Romaka et al.,[12] and the β-LnNi$_{1-x}$Ga$_4$ (Ln = Tb – Er, open circles) series as obtained from this work. α-LnNiGa$_4$ (Ln = Gd – Tm) corresponds to the upper (x) and right (y) axis while β-LnNiGa$_4$ (Ln = Tb – Er) corresponds to the lower (x) and left (y) axis.

The field dependence of the magnetization at 3 K for each of the β-LnNi$_{1-x}$Ga$_4$ analogues is shown in Figure 6. The expected saturated moment for a free Tb^{3+} ion is 9.0 μ_B/mol. β-TbNi$_{0.9(1)}$Ga$_4$ did not saturate in an applied field up to 9 T and reached a maximum value of approximately 3.3 μ_B/mol. The absence of saturation is common for an antiferromagnetic compound. Similarly, the magnetization of β-DyNi$_{0.9(1)}$Ga$_4$ increased linearly up to 5 T, at which point a decrease in slope was observed. For the applied fields of 5 T < H < 9 T for β-DyNi$_{0.9(1)}$Ga$_4$, a linear increase was observed with a maximum saturated moment of 5.6 μ_B/mol at 9 T (μ_{sat} = 10.0 μ_B/mol for Dy^{3+}). β-HoNi$_{0.9(1)}$Ga$_4$ did not order magnetically down to 2 K, as was noted from the magnetic susceptibility. This was reinforced by the magnetization data collected at 3 K. The magnetization of β-HoNi$_{0.9(1)}$Ga$_4$ was linear at the low applied fields (H < 3 T) but when fields larger than 3 T were applied a change in the slope was observed, which is indicative of the onset of spin saturation in a paramagnet. A maximum value of 6.5 μ_B/mol at 9 T was recovered (μ_{sat} = 10.0 μ_B/mol for Ho^{3+}). Under a low applied field, the magnetization of β-ErNi$_{0.8(1)}$Ga$_4$ was very similar to that of β-HoNi$_{0.9(1)}$Ga$_4$, namely, linear magnetization. A change in the slope was observed when an external field that was greater than 2 T was applied and a maximum of approximately 4.9 μ_B/mol at 9 T was obtained.

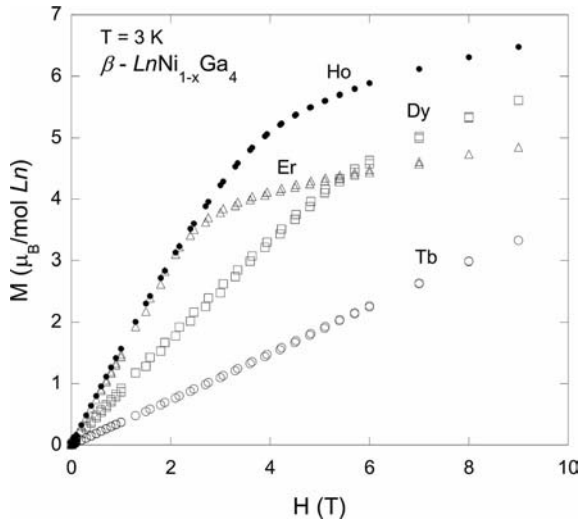

Figure 6. The isothermal magnetization of β-TbNi$_{0.9(1)}$Ga$_4$ (open circles), β-DyNi$_{0.9(1)}$Ga$_4$ (open squares), β-HoNi$_{0.9(1)}$Ga$_4$ (closed circles), and β-ErNi$_{0.8(1)}$Ga$_4$ (open triangles) as a function of the applied field at T = 3 K. The data were recorded while sweeping between 0 and 9 T.

The resistance data for β-LnNi$_{1-x}$Ga$_4$ (Ln = Tb–Er) is shown in Figure 7 (with β-ErNi$_{0.8(1)}$Ga$_4$ shown in the inset). All of the analogues display metallic behavior down to 3 K. The RRR values [ρ(290 K)/ρ(3 K)] of 3.8, 2.0, 1.4, and 6.0 for the Tb, Dy, Ho, and Er analogues, respectively, are fairly small and attest to the structural disorder. In addition, the positive magnetoresistance {MR = [$\rho(H) - \rho(H = 0)$]/$\rho(H = 0)$} that was measured as 26, 17, 12, and 67% for the Tb, Dy, Ho, and Er β-LnNi$_{1-x}$Ga$_4$ analogues at 9 T, respectively, is indicative of a classical mechanism for Tb, Dy, and Ho, while the Er sample showed enhanced scattering upon application of an external field (the Er sample also showed the largest RRR value).

The resistivity data for the α-LnNi$_{0.9(1)}$Ga$_4$ (Ln = Y, Gd – Tm) series is shown in Figure 8. All of the analogues show metallic behavior at a low temperature, the Tm analogue showed metallic behavior down to 5 K. However, the Er analogue did not follow the linear trend of the Ho ana-

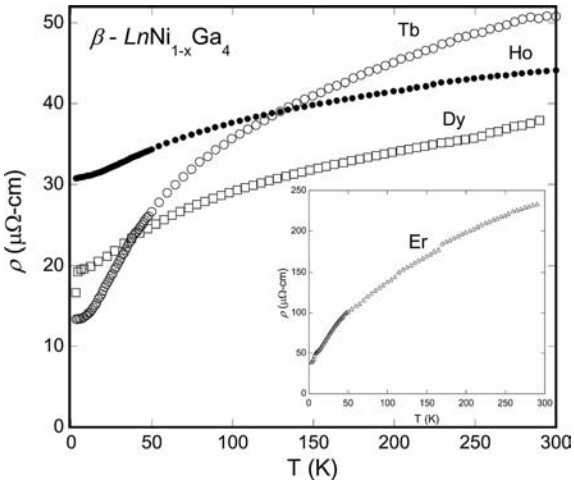

Figure 7. The electrical resistance of β-$TbNi_{0.9(1)}Ga_4$ (open circles), β-$DyNi_{0.9(1)}Ga_4$ (open squares), β-$HoNi_{0.9(1)}Ga_4$ (closed circles), and β-$ErNi_{0.8(1)}Ga_4$ (open triangles, inset) as a function of temperature.

logue up to 3 T. The RRR values of 3.6, 3.6, 3.6, 4.3, 3.9, 3.3, and 2.7 were found for Y and Gd–Tm, respectively. α-$DyNi_{0.9(1)}Ga_4$ had the largest positive MR value (32%) at 9 T. The α-$LnNiGa_4$ analogues were similar to β-$LnNi_{1-x}Ga_4$ and showed small values for the MR, which is indicative of a classical scattering mechanism upon the application of an external field.

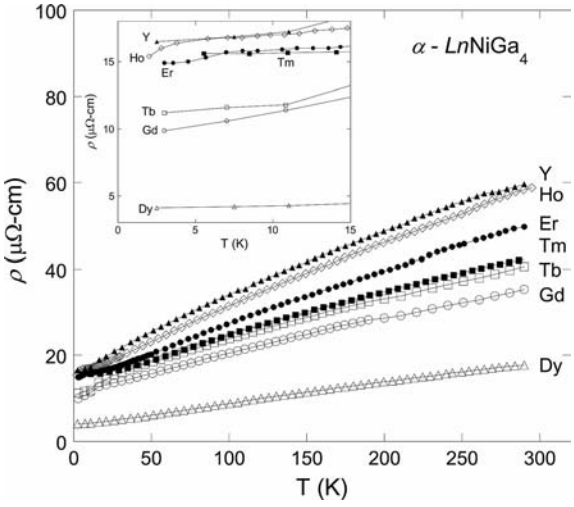

Figure 8. The electrical resistivity of α-$GdNiGa_4$ (open circles), α-$TbNiGa_4$ (open squares), α-$DyNiGa_4$ (open triangles), α-$HoNiGa_4$ (open diamonds), α-$ErNiGa_4$ (closed circles), α-$TmNiGa_4$ (closed squares), and α-$YNiGa_4$ (closed triangles) as a function of temperature. The low temperature resistivity is shown in the inset for the purpose of clarity.

Conclusions

We have successfully grown two polymorphs of $LnNiGa_4$ (α and β). β-$LnNi_{1-x}Ga_4$ (Ln = Tb–Er), which is a defect variant of the Ce_2NiGa_{10}-structure type,[14] is isotypic to $LnNiGa_3Ge$ (Ln = Y, Sm, Gd, Tb, Er, Tm)[19] and has an additional split Ga site. The structural distortion found in β-$LnNi_{1-x}Ga_4$ (Ln = Tb–Er) could be attributed to the Ni occupation at the 4*e* site, which induces a distortion in the surrounding Ga environment. We have reported, for the first time, the magnetic properties of β-$LnNi_{1-x}Ga_4$ (Ln = Tb–Er) and the transport properties of β-$LnNi_{1-x}Ga_4$ (Ln = Tb–Er) and α-$LnNiGa_4$ (Ln = Gd – Tm). The magnetic moments that were obtained for β-$LnNi_{1-x}Ga_4$ (Ln = Tb–Er) from the Curie–Weiss fits are consistent with the trivalent lanthanide moment and, interestingly, the θ_W for both α-$LnNiGa_4$ (Ln = Gd – Tm)[12] and β-$LnNi_{1-x}Ga_4$ (Ln = Tb–Er) scale as a function of the de Gennes factor.

Experimental Section

Synthesis of α-$LnNiGa_4$ (Ln = Y, Gd–Yb) and β-$LnNi_{1-x}Ga_4$ (Ln = Tb–Er): The single-crystals of the two polymorphs, orthorhombic α-$LnNiGa_4$ (Ln = Y, Gd–Yb) and tetragonal β-$LnNi_{1-x}Ga_4$ (Ln = Tb–Er), were grown by using the self-flux method where Ln (3*N*, Alfa Aesar), Ni powder (5*N*, Alfa Aesar), and Ga shot (7*N*, Alfa Aesar) were placed into the alumina crucibles in a 1.5:1:15 mol ratio. The only exception to this prescribed mol ratio was the Tm analogue, which required a 2:1:15 stoichiometric ratio of Tm/Ni/Ga in order to grow large crystals of α-$TmNiGa_4$. The previous stoichiometric ratio yielded smaller crystals of α-$TmNiGa_4$, which were approximately 2 mm in length. Each crucible was covered with quartz wool, sealed in an evacuated silica tube, and placed into a high temperature furnace for the heat treatment.

X-ray Crystallographic Studies: Several crystals of both the α-$LnNiGa_4$ (Ln = Y, Gd–Yb) and β-$LnNi_{1-x}Ga_4$ (Ln = Tb–Er) phases were ground in order to be used for characterization by X-ray powder diffraction with a Bruker AXS D8 Advance diffractometer in order to confirm the phase purity. The powder X-ray diffraction patterns from the different batches were also compared with one another in order to confirm the phase purity. Independent powder diffraction on the rods or plates confirmed the phase purity of α-$LnNiGa_4$ (Ln = Y, Gd–Yb) and β-$LnNi_{1-x}Ga_4$ (Ln = Tb–Er), respectively, and indicated that the α and β-phases can be separated by means of the crystal morphology. Silver-colored fragments of α-$LnNiGa_4$ (Ln = Y, Gd–Yb) and β-$LnNi_{1-x}Ga_4$ (Ln = Tb–Er), which had approximate dimensions of $0.03 \times 0.03 \times 0.04$ mm^3, were cleaved from the single-crystals and were mounted on the goniometer of a Nonius Kappa CCD diffractometer that was equipped with Mo-K_α radiation (λ = 0.71073 Å). The data were collected up to θ = 30° at 298 K for α-$LnNiGa_4$ (Ln = Y, Gd–Yb) and the data were collected up to θ = 31° at 100 K for β-$LnNi_{1-x}Ga_4$ (Ln = Tb–Er). SIR92[37] was used to obtain a starting model for all of the samples and SHELXL-97[38] was used for the structure refinement. The data for all of the samples were corrected for absorption and extinction, and were refined with anisotropic displacement parameters, except for the Ga5 position in β-$LnNi_{1-x}Ga_4$ (Ln = Tb–Er), which was refined with isotropic displacement parameters. All of the refinement models were checked for missing symmetry elements by using PLATON.[39] The crystallographic data are presented in Tables 7 and 8 for α-$LnNiGa_4$ (Ln = Y, Gd–Yb) and Table 9 for β-$LnNi_{1-x}Ga_4$ (Ln = Tb–Er).

Table 7. Crystallographic data for α-LnNiGa$_4$ (Ln = Y, Gd – Dy), orthorhombic, *Cmcm*.

Composition	α-YNiGa$_4$	α-GdNiGa$_4$	α-TbNiGa$_4$	α-DyNiGa$_4$
a [Å]	4.076(5)	4.093(5)	4.080(5)	4.069(5)
b [Å]	15.245(5)	15.355(5)	15.286(5)	15.230(5)
c [Å]	6.552(5)	6.548(5)	6.542(5)	6.529(5)
V [Å^3]	407.1(6)	411.5(6)	408.0(6)	404.6(6)
Z	4	4	4	4
Size [mm^3]	0.03 × 0.03 × 0.05	0.03 × 0.03 × 0.05	0.03 × 0.03 × 0.04	0.03 × 0.03 × 0.05
θ range [°]	2.67–30.04	2.65–29.95	4.10–29.99	2.67–30.04
μ [mm^{-1}]	44.477	45.946	47.421	48.808
Temperature [K]	298(2)	298(2)	298(2)	298(2)
Reflections with $I > 2\sigma(I)$	363	363	363	361
R_{int}	0.0242	0.0256	0.0221	0.0362
h	–5 → 5	–5 → 5	–5 → 5	–5 → 5
k	–21 → 21	–21 → 21	–20 → 21	–19 →21
l	–9 → 9	–9 → 9	–9 → 9	–8 → 9
$R_1[F^2 > 2\sigma(F^2)]$[a]	0.0362	0.0282	0.0284	0.0398
$wR_2(F^2)$[b]	0.0870	0.0695	0.0722	0.0989
Parameters	24	24	24	24
GooF	1.168	1.1085	1.207	1.111
$\Delta\rho_{max}$ [e/Å^3]	1.606	2.542	2.228	2.883
$\Delta\rho_{min}$ [e/Å^3]	–3.220	–2.349	–2.695	–2.544
Extinction coeff.	0.0109(10)	0.0043(4)	0.0117(7)	0.0042(5)

[a] $R_1 = \Sigma||F_o| - |F_c||/\Sigma|F_o|$. [b] $wR_2 = \{\Sigma[w(F_o^2 - F_c^2)^2]/\Sigma[w(F_o^2)^2]\}^{1/2}$; $w = 1/[\sigma^2F_o^2 + (0.0473P)^2 + 4.6268P]$, $w = 1/[\sigma^2F_o^2 + (0.0332P)^2 + 8.3260P]$, $w = 1/[\sigma^2F_o^2 + (0.0304P)^2 + 4.3163P]$, and $w = 1/[\sigma^2F_o^2 + (0.0538P)^2 + 11.0962P]$ for YNiGa$_4$, GdNiGa$_4$, TbNiGa$_4$, and DyNiGa$_4$, respectively.

Table 8. Crystallographic data for α-LnNiGa$_4$ (Ln = Ho – Tm), orthorhombic, *Cmcm*.

Composition	α-HoNiGa$_4$	α-ErNiGa$_4$	α-TmNiGa$_4$	α-YbNiGa$_4$
a [Å]	4.062(5)	4.057(4)	4.0478(4)	4.0850(4)
b [Å]	15.185(5)	15.140(5)	15.0883(7)	15.2900(14)
c [Å]	6.534(5)	6.537(5)	6.5517(4)	6.4980(6)
V [Å^3]	403.0(6)	401.5(5)	400.14(4)	405.86(7)
Z	4	4	4	4
Size [mm^3]	0.03 × 0.05 × 0.05	0.03 × 0.03 × 0.05	0.05 × 0.05 × 0.08	00.02 × 0.03 × 0.04
θ range [°]	2.68–29.98	4.12–29.96	2.70–29.96	4.12–30.08
μ [mm^{-1}]	50.091	51.474	52.851	53.289
Temperature [K]	298(2)	298(2)	298(2)	298(2)
Reflections with $I > 2\sigma(I)$	360	355	357	363
R_{int}	0.0300	0.0203	0.0370	0.0354
h	–5 → 5	–5 → 5	–5 → 5	–5 → 5
k	–19 → 21	–19 → 20	–19 → 20	–21 → 20
l	–9 → 9	–9 → 9	–9 → 9	–8 → 9
$R_1[F^2 > 2\sigma(F^2)]$[a]	0.0300	0.0463	0.0343	0.0433
$wR_2(F^2)$[b]	0.0691	0.1162	0.0912	0.1085
Parameters	24	24	24	24
GooF	1.167	1.264	1.125	1.103
$\Delta\rho_{max}$ [e/Å^3]	1.824	3.732	3.829	4.301
$\Delta\rho_{min}$ [e/Å^3]	–2.536	–3.678	–2.496	–4.455
Extinction coeff.	0.0041(3)	0.0048(3)	0.0047(5)	0.0075(8)

[a] $R_1 = \Sigma||F_o| - |F_c||/\Sigma|F_o|$. [b] $wR_2 = \{\Sigma[w(F_o^2 - F_c^2)^2]/\Sigma[w(F_o^2)^2]\}^{1/2}$; $w = 1/[\sigma^2F_o^2 + (0.0253P)^2 + 4.2528P]$, $w = 1/[\sigma^2F_o^2 + (0.0703P)^2 + 4.0443P]$, $w = 1/[\sigma^2F_o^2 + (0.0453P)^2 + 21.3808P]$, and $w = 1/[\sigma^2F_o^2 + (0.0643P)^2 + 10.4431P]$ for HoNiGa$_4$, ErNiGa$_4$, TmNiGa$_4$, and YbNiGa$_4$, respectively.

Further details on the crystal structure investigations may be obtained from the Fachinformationszentrum Karlsruhe, 76344 Eggenstein-Leopoldshafen, Germany (fax: +49-7247-808-666; e-mail: crysdata@fiz-karlsruhe.de), on quoting the depository numbers CSD-423074 (for α-YNiGa$_4$), -423067 (for α-GdNiGa$_4$), -423068 (for α-TbNiGa$_4$), -423065 (for α-DyNiGa$_4$), -423079 (for α-HoNiGa$_4$), -423066 (for α-ErNiGa$_4$), -423069 (for α-TmNiGa$_4$), -423070 (for α-YbNiGa$_4$), -423073 (for β-TbNi$_{0.9(1)}$Ga$_4$), -423071 (for β-DyNi$_{0.9(1)}$Ga$_4$), -423072 (for β-HoNi$_{0.9(1)}$Ga$_4$), and -423078 (for β-ErNi$_{0.8(1)}$Ga$_4$).

Elemental Analysis: A Hitachi S-3600N scanning electron microscope with an energy dispersive X-ray spectrometer (SEM-EDXS) was used to analyze the elemental content of the single-crystals of α-LnNiGa$_4$ (Ln = Y, Gd–Yb) and β-LnNi$_{1-x}$Ga$_4$ (Ln = Tb–Er). The experimental parameters included an accelerating voltage of 15 kV and a beam-to-sample distance of 15 mm. Several of the crystals from the multiple growths were scanned at 5 areas/crystal for 50 seconds/area. The average composition was normalized to Ln (Ln = lanthanide) in order to yield LnNi$_{0.95(4)}$Ga$_{4.0(1)}$ for α-LnNiGa$_4$ (Ln = Y, Gd–Yb), LnNi$_{0.9(1)}$Ga$_{4.0(1)}$ for β-LnNi$_{1-x}$Ga$_4$

Table 9. Crystallographic data for β-$LnNi_{1-x}Ga_4$ (Ln = Tb–Er), tetragonal, *I*4/*mmm*.

Composition	β-$TbNi_{0.9(1)}Ga_4$	β-$DyNi_{0.9(1)}Ga_4$	β-$HoNi_{0.9(1)}Ga_4$	β-$ErNi_{0.8(1)}Ga_4$
a [Å]	4.1980(6)	4.1790(6)	4.1680(2)	4.1620(6)
c [Å]	23.7890(14)	23.6450(16)	23.5370(14)	23.4650(16)
V [Å^3]	419.24(9)	412.94(2)	408.89(4)	406.47(9)
Z	4	4	4	4
Size [mm^3]	0.03 × 0.03 × 0.04	0.03 × 0.03 × 0.04	0.03 × 0.03 × 0.02	0.03 × 0.03 × 0.03
θ range [°]	3.43–29.81	3.45–29.97	3.46–30.92	3.47–30.99
μ [mm^{-1}]	45.845	47.513	49.060	50.038
Temperature [K]	100(2)	100(2)	100(2)	100(2)
Reflections with $I > 2\sigma(I)$	224	223	241	229
R_{int}	0.0174	0.0201	0.0273	0.0250
h	–5 → 5	–5 → 5	–5 → 6	–6 → 6
k	–4 → 4	–4 → 5	–5 → 6	–4 → 6
l	–32 → 32	–32 → 32	–34 → 33	–32 → 33
$R_1[F^2 > 2\sigma F^2]$[a]	0.0452	0.0295	0.0370	0.0284
$wR_2(F^2)$[b]	0.1226	0.0807	0.1008	0.0792
Parameters	25	25	25	25
GooF	1.141	1.134	1.158	1.204
Δp_{max} [e/Å^3]	4.057	2.954	2.869	2.209
Δp_{min} [e/Å^3]	–2.302	–1.968	–1.523	–1.905
Extinction coeff.	0.0030(8)	0.0075(8)	0.0061(9)	0.0099(9)

[a] $R_1 = \Sigma||F_o| - |F_c||/\Sigma|F_o|$. [b] $wR_2 = [\Sigma w(F_o^2 - F_c^2)^2/\Sigma w(F_o^2)^2]^{1/2}$; $w = 1/[\sigma^2(F_o^2) + (0.0833P)^2 + 16.5470P]$, $w = 1/[\sigma^2(F_o^2) + (0.0408P)^2 + 13.7110P]$, $w = 1/[\sigma^2(F_o^2) + (0.0574P)^2 + 13.3851P]$, and $w = 1/[\sigma^2(F_o^2) + (0.0432P)^2 + 9.6559P]$ at 100 K for β-$TbNi_{0.9(1)}Ga_4$, β-$DyNi_{0.9(1)}Ga_4$, β-$HoNi_{0.9(1)}Ga_4$, and β-$ErNi_{0.8(1)}Ga_4$, respectively.

(Ln = Tb–Ho), and $ErNi_{0.8(1)}Ga_{4.0(1)}$ for β-$ErNi_{1-x}Ga_4$. The composition of each of the phases that were obtained by SEM analysis was consistent, within error, with the refined composition that was determined by the single-crystal X-ray diffraction studies.

Magnetic and Transport Property Measurements: The magnetization data for β-$LnNi_{1-x}Ga_4$ (Ln = Tb–Er) were obtained with a Quantum Design Physical Property Measurement System. The temperature-dependent magnetization was measured under zero-field cooled conditions from 2 to 300 K with an applied field 0.1 T. The field-dependent magnetization was measured at 3 K by sweeping between 0 and 9 T. The electrical resistivity and resistance was measured for α-$LnNiGa_4$ (Ln = Y, Gd–Tm) and β-$LnNi_{1-x}Ga_4$ (Ln = Tb–Er), respectively, with the standard four-probe AC technique from 3 to 300 K at 27 Hz with excitation currents of approximately 0.5 mA.

Acknowledgments

J. F. D., D. P. Y., and J. Y. C. acknowledge support from the National Science Foundation (NSF) through DMR0804376, DMR0449022, and DMR0756281, respectively.

[1] D. L. Gray, M. C. Francisco, M. G. Kanatzidis, *Inorg. Chem.* **2008**, *47*, 7243–7248.
[2] M. A. Zhuravleva, M. Evain, V. Petricek, M. G. Kanatzidis, *J. Am. Chem. Soc.* **2007**, *129*, 3082–3083.
[3] R. Troc, P. Rogl, V. H. Tran, A. Czopnik, *J. Solid State Chem.* **2001**, *158*, 227–235.
[4] J. R. Salvador, F. Guo, T. Hogan, M. G. Kanatzidis, *Nature* **2003**, *425*, 702–705.
[5] S. Margadonna, K. Prassides, A. N. Fitch, J. R. Salvador, M. G. Kanatzidis, *J. Am. Chem. Soc.* **2004**, *126*, 4498–4499.
[6] M. C. Menard, Y. Xiong, A. B. Karki, B. L. Drake, P. W. Adams, F. R. Fronczek, D. P. Young, J. Y. Chan, *J. Solid State Chem.* **2010**, *183*, 1935–1942.
[7] J. S. Hwang, K. J. Lin, C. Tien, *Solid State Commun.* **1996**, *100*, 169–172.
[8] C. Tien, C. H. Feng, C. S. Wur, J. J. Lu, *Phys. Rev. B* **2000**, *61*, 12151.
[9] B. L. Drake, M. J. Kangas, C. Capan, N. Haldolaarachchige, Y. Xiong, P. W. Adams, D. P. Young, J. Y. Chan, *J. Phys. Condens. Matter* **2010**, *22*, 426002.
[10] S. A. M. Mentink, G. J. Nieuwenhuys, A. A. Menovsky, J. A. Mydosh, H. Tou, Y. Kitaoka, *Phys. Rev. B* **1994**, *49*, 15759–15763.
[11] X. Z. Chen, P. Small, S. Sportouch, M. Zhuravleva, P. Brazis, C. R. Kannewurf, M. G. Kanatzidis, *Chem. Mater.* **2000**, *12*, 2520–2522.
[12] V. A. Romaka, Y. N. Grin, Y. P. Yarmolyuk, *Ukr. Fiz. Zh.* **1983**, *28*, 1095–1097.
[13] R. M. Rykhal, O. S. Zarechnyuk, Y. P. Yarmolyuk, *Sov. Phys. Crystallogr.* **1972**, *17*, 453–455.
[14] Y. P. Yarmolyuk, Y. N. Grin, I. V. Rozhdestvenskaya, O. A. Usov, A. M. Kuzmin, V. A. Bruskov, E. I. Gladyshevskij, *Kristallografiya* **1982**, *27*, 599–600.
[15] K. R. Thomas, J. Y. Cho, J. N. Millican, R. D. Hembree, M. Moldovan, A. Karki, D. P. Young, J. Y. Chan, *J. Cryst. Growth* **2010**, *312*, 1098–1103.
[16] Y. Grin, K. Hiebl, P. Rogl, *J. Less-Common Met.* **1990**, *162*, 361–369.
[17] L. Vasylechko, W. Schnelle, M. Schmidt, U. Burkhardt, H. Borrmann, U. Schwarz, Y. N. Grin, *J. Alloys Compd.* **2006**, *416*, 35–42.
[18] J. Pelleg, G. Kimmel, D. Dayan, *J. Less-Common Met.* **1981**, *81*, 33–44.
[19] M. A. Zhuravleva, R. J. Pcionek, X. Wang, A. J. Schultz, M. G. Kanatzidis, *Inorg. Chem.* **2003**, *42*, 6412–6424.
[20] E. Parthe, *Modern Perspectives in Inorganic Chemistry*, Kluwer Academic Publishers, Boston, **1992**.
[21] Y. Grin, Y. P. Yarmolyuk, E. I. Gladyshevskii, *Sov. Phys. Crystallogr.* **1982**, *27*, 413–417.
[22] B. Sieve, P. N. Trikalitis, M. G. Kanatzidis, *Z. Anorg. Allg. Chem.* **2002**, *628*, 1568–1574.
[23] S. Cirafici, E. Franceschi, *J. Less-Common Met.* **1981**, *77*, 269–280.
[24] A. Palenzona, E. Franceschi, *J. Less-Common Met.* **1968**, *14*, 47–53.
[25] S. E. Haszko, *T. Metall. Soc. Aime.* **1961**, *221*, 201.

[26] J. Emsley, *The Elements*, Oxford University Press, New York, **1998**.
[27] E. Hellner, *Z. Metallkd.* **1950**, *41*, 480–484.
[28] S. Bhan, K. Schubert, *J. Less-Common Met.* **1974**, *36*, 15–30.
[29] M. Ellner, S. Bhan, K. Schubert, *J. Less-Common Met.* **1969**, *19*, 245–252.
[30] E. Haeussermann, M. Elding-Ponten, C. Svensson, S. Lidin, *Chem. Eur. J.* **1998**, *4*, 1007–1015.
[31] C. Schmetterer, H. Flandorfer, C. L. Lengauer, J.-P. Bros, H. Ipser, *Intermetallics* **2010**, *18*, 277–285.
[32] Y. N. Grin, Y. P. Yarmolyuk, I. V. Rozhdestvenskaia, *Sov. Phys. Crystallogr.* **1983**, *28*, 477–479.
[33] Y. N. Grin, Y. P. Yarmolyuk, O. A. Usov, A. M. Kuz′min, V. A. Bruskov, *Sov. Phys. Crystallogr.* **1983**, *28*, 710–711.
[34] X. Z. Chen, S. Sportouch, B. Sieve, P. Brazis, C. R. Kannewurf, J. A. Cowen, R. Patschke, M. G. Kanatzidis, *Chem. Mater.* **1998**, *10*, 3202–3211.
[35] R. Giedigkeit, R. Niewa, W. Schnelle, Y. Grin, R. Kniep, *Z. Anorg. Allg. Chem.* **2002**, *628*, 1692–1696.
[36] J. E. Greedan, *J. Mater. Chem.* **2001**, *11*, 37–53.
[37] A. Altomare, M. C. Burla, M. Camalli, G. Cascarano, C. Giacovazzo, A. Guagliardi, G. Polidori, *J. Appl. Crystallogr.* **1994**, *27*, 435.
[38] G. M. Sheldrick, *Acta Crystallogr., Sect. A* **2008**, *64*, 112–122.
[39] A. L. Spek, *J. Appl. Crystallogr.* **2003**, *36*, 7–13.

Received: March 22, 2011
Published Online: July 4, 2011
Minor changes have been made since publication in Early View.

